ChemSusChem

Research Article
doi.org/10.1002/cssc.202301170

Chemistry Europe
European Chemical Societies Publishing

www.chemsuschem.org

Donor-Acceptor Conjugated Acetylenic Polymers for High-Performance Bifunctional Photoelectrodes

Mino Borrelli,[a] Yun An,[b, c] Christine Joy Querebillo,[a, d] Ahiud Morag,[a, e] Christof Neumann,[f] Andrey Turchanin,[f] Hanjun Sun,[g] Agnieszka Kuc,[h, i] Inez M. Weidinger,*[a] and Xinliang Feng*[a, e]

Due to the drastic required thermodynamical requirements, a photoelectrode material that can function as both a photocathode and a photoanode remains elusive. In this work, we demonstrate for the first time that, under simulated solar light and without co-catalysts, donor-acceptor conjugated acetylenic polymers (CAPs) exhibit both impressive oxygen evolution (OER) and hydrogen evolution (HER) photocurrents in alkaline and neutral medium, respectively. In particular, poly(2,4,6-tris(4-ethynylphenyl)-1,3,5-triazine) (**pTET**) provides a benchmark OER photocurrent density of ~200 $\mu A\,cm^{-2}$ at 1.23 V vs. reversible hydrogen electrode (RHE) at pH 13 and a remarkable HER photocurrent density of ~190 $\mu A\,cm^{-2}$ at 0.3 V vs. RHE at pH 6.8. By combining theoretical investigations and electrochemical-operando Resonance Raman spectroscopy, we show that the OER proceeds with two different mechanisms, with the electron-depleted triple bonds acting as single-site OER in combination with the C4-C5 atoms of the phenyl rings as dual sites. The HER, instead, occurs via an electron transfer from the tri-acetylenic linkages to the triazine rings, which act as the HER active sites. This work represents a novel application of organic-based materials and contributes to the development of high-performance photoelectrochemical catalysts for the solar fuels' generation.

Introduction

The depletion of fossil fuels, their negative impact on the environment, and the lack of economically-viable energy alternatives are issues of uttermost importance in the current energy crisis.[1] Photoelectrochemical (PEC) water splitting into its gaseous components is a highly appealing technology for hydrogen production thanks to the utilization of inexhaustible solar energy and water as feedstock.[2–3] Since the pioneering discovery of water photolysis by TiO_2,[4] inorganic materials, such as metal oxides,[5–9] transition-metal dichalcogenides,[10–11] and metal sulphides[12–13] have been widely employed as photoelectrode materials. However, their electronic structures make them suitable for only one of the two half-reactions, the hydrogen evolution reaction (HER) or the oxygen evolution reaction (OER). As a consequence, to complete the whole water splitting cycle, two different photoelectrodes with or without bias are generally utilized.[14–17] Conjugated polymers, constituted by a delocalized π-system, present tunable energy levels (and absorption profiles), atomic-level active site modulation, and facile and low-cost synthetic procedures.[18] Moreover, they are intrinsically ambipolar,[19–20] able to transport both electrons and holes, and therefore are excellent candidates to allow the overall water splitting with the same electrode, thus reducing

[a] *Dr. M. Borrelli, Dr. C. J. Querebillo, Dr. A. Morag, Prof. Dr. I. M. Weidinger, Prof. Dr. X. Feng*
Department of Chemistry and Food Chemistry and Center of Advancing Electronics Dresden (cfaed)
Technische Universität Dresden
Mommsenstrasse 4, 01062 Dresden (Germany)
E-mail: inez.weidinger@tu-dresden.de
xinliang.feng@tu-dresden.de

[b] *Dr. Y. An*
Helmholtz-Zentrum Dresden-Rossendorf
Permoserstraße 15, 04318 Leipzig (Germany)

[c] *Dr. Y. An*
Beijing Key Laboratory of Theory and Technology for Advanced Batteries Materials, School of Materials Science and Engineering, Peking University
100871 Beijing (China)

[d] *Dr. C. J. Querebillo*
Leibniz-Institute for Solid State and Materials Research (IFW)
Helmholtzstrasse 20, 01069 Dresden (Germany)

[e] *Dr. A. Morag, Prof. Dr. X. Feng*
Department of Synthetic Materials and Functional Devices
Max-Planck Institute of Microstructure Physics
Weinberg 2, 06120 Halle (Germany)

[f] *Dr. C. Neumann, Prof. Dr. A. Turchanin*
Institute of Physical Chemistry and Center for Energy and Environmental Chemistry Jena (CEEC Jena)
Friedrich Schiller University Jena
Lessingstrasse 10, 07743 Jena (Germany)

[g] *Prof. Dr. H. Sun*
School of Chemistry and Materials Science
Nanjing Normal University
1 Wenyuan Road, Nanjing 210023 (China)

[h] *Dr. A. Kuc*
Helmholtz-Zentrum Dresden-Rossendorf
Bautzner Landstr. 400, 01328 Dresden (Germany)

[i] *Dr. A. Kuc*
Centrum for Advanced Systems Understanding, CASUS
Untermarkt 20, 02826 Görlitz (Germany)

Supporting information for this article is available on the WWW under https://doi.org/10.1002/cssc.202301170

the costs and simplifying the cell design. Up to now, there are neither organic nor inorganic photoelectrodes capable of producing both hydrogen and oxygen. The reason lies in the challenging thermodynamic requirements: the conduction band (CB) and the valence band (VB) must be above the HER level and below the OER level, respectively. Furthermore, ambipolarity, proper bandgaps, and active sites for both half-reactions are required. Driven by the above considerations, herein we demonstrate the unprecedented use of novel conjugated acetylenic polymers (CAPs) as both photoanodes and photocathodes. By increasing the donor-acceptor character from poly(1,3,5-triethynylbenzene) (**pTEB**) and poly(4,4″-diethynyl-5′-(4-ethynylphenyl)-1,1′:3′,1″-terphenyl) (**pTETH**) to poly(2,4,6-tris(4-ethynylphenyl)-1,3,5-triazine) (**pTET**), remarkable hydrogen evolution and oxygen evolution photocurrents of ~190 $\mu A\,cm^{-2}$ (at 0.3 V vs. RHE) and ~200 $\mu A\,cm^{-2}$ (at 1.23 V vs. RHE) are detected in neutral (pH 6.8) and alkaline (pH 13.0) solutions, respectively (Figure 1a). Electrochemical-operando resonance Raman spectroscopy and density functional theory (DFT) investigations elucidate the catalytic mechanisms of **pTET**. A photoinduced electron transfer, from the donor-rich triple bonds of the triacetylenic linkages to the acceptor N atoms of the triazine, enriches the latter into becoming HER active sites, while the electron-depleted triple bonds can act as OER single-site. Although less favourably predicted by DFT, the sp^2-carbon atoms of the phenyl units in **pTET** can also undergo dual-site OER, as revealed by the vibrational spectroelectrochemistry. Our work represents a new pathway of organic-based materials and contributes to the development of high-performance photoelectrochemical catalysts for the solar fuels' generation.

Results and Discussion

The CAPs were synthesized on commercial Cu foams via a Glaser-type polymerization with the Cu substrates functioning as catalysts and current collectors, following the previously reported procedure[21–22] (SI). A densely-interconnected nanosheet layer, which is the typical CAPs morphology, was observed using scanning electrode microscopy (SEM) (Figure 1b and Figure S1). X-ray photoelectron spectroscopy (XPS) and resonance Raman (RR) spectroscopy studies were conducted to confirm the polymerization and provide chemical information. The deconvolution of the high-resolution C1s core level XP spectra show the *sp*-carbon signal of **pTET** and **pTETH** at 283.5 eV and 283.7 eV, respectively; whereas the reported value for **pTEB** is slightly higher (283.8 eV) (Figures S2-S3).[23] In the RR spectra, characteristic peaks can be assigned as follows: –C≡C– stretching of the triacetylenic linkages (at 2209~2221 cm^{-1}), aromatic ring stretches at 1490~1610 cm^{-1}, ring deformation modes at 1500~1590 cm^{-1}, shear vibrational modes at 1130~1190 cm^{-1}, and ring breathing modes at 990~1420 cm^{-1} (Figure S4). The band shift pertaining to the –C≡C– stretch follows the trend: **pTET** < **pTETH** < **pTEB**. We previously demonstrated that, in thiophene-based CAPs, this value is related to the HER catalytic activity.[22] The different shifts of the –C≡C– stretch in **pTET** (2209 cm^{-1}) and poly(2,5-diethynylthieno[3,2-b]thiophene) **pDET** (2170 cm^{-1}; Figure S5) points to the different electronic structures of the two polymers. **pDET**, being electron-rich, boosts the electron density of the adjacent triple bonds, thus weakening its bonds (2170 cm^{-1}), while the 2,4,6-triphenyl-1,3,5-triazine moieties of **pTET**, attracting electrons from the electron-rich(er) triple bonds, deplete them and strengthening their bond energy (2209 cm^{-1}). The optoelectronic properties of the CAPs were investigated using ultraviolet-visible absorption spectroscopy (UV-Vis) and ultraviolet photoelectron spectroscopy (UPS). The absorption profiles of the CAPs on Cu foils were measured in reflectance mode. Furthermore, the reflectance spectra of the CAPs on the Cu foils were converted to absorbance, assuming that in absence of any transmitted light, the sum of reflectance and absorbance is unity (Figure S6). The additional bands visible in the spectral window of 550–600 nm arise from Cu plasmonic bands.[24] **pTEB** and **pTETH** show the same features, while **pTET** has an earlier absorption edge (558 nm) and a red-shifted maximum (495 nm; Figure 1c). Consequently, the Tauc plots (Figure S7) reveal the smallest bandgap of 2.29 eV for **pTET**, followed by **pTEB** (2.32 eV) and **pTETH** (2.42 eV). The VB positions of the CAPs were determined via UPS at ca. −6.33, -6.40, and −6.63 eV for **pTET**, **pTETH**, and **pTEB**, respectively. Combining the VB values from UPS and the optical bandgap (E_g) energies from UV-Vis, the CB values, calculated according to the formula $E_{CB} = E_{VB} + E_g$ (in eV), were derived to be −4.04, −3.98, and −4.12 eV for **pTET**, **pTETH**, and **pTEB**, respectively (Figure S8). The electronic structures of the CAPs, illustrated in Figure 1d, can satisfy the thermodynamical requirements for both HER and OER reported in their standard potentials (0 V and 1.23 V vs. normal hydrogen electrode, NHE, respectively). In order to investigate the OER activity, a new support had to be synthesized because the previously used Cu foams[22] could not serve as a current collector at anodic potentials due to the high currents generated by Cu oxidation.[25] A possible way to overcome this obstacle was the synthesis of NiCu-dendritic deposition on Ni foil/foam(SI).[26]

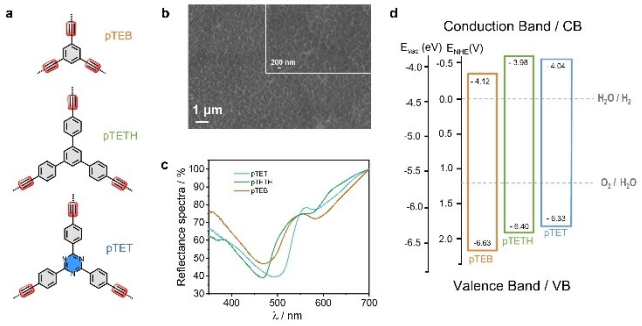

Figure 1. Chemical structures of the CAPs and characterization. a) Chemical structure of the conjugated acetylenic polymers. b) Typical SEM image of **pTET**/Cu foam at different magnifications. c) Reflectance spectra of the CAPs on Cu foil. d) Summary of the optoelectronic properties and thermodynamical HER and OER energy levels.

This approach provides dense Cu sites which is crucial to enable the in-situ Glaser-type polymerization and a limited (dark) electrochemical response, as confirmed by SEM and

energy dispersive X-ray spectroscopy (EDS; Figure S9). X-ray diffraction (XRD) was employed to detect the surface modification of the NiCu support (Figure S10). The XRD peaks at 43.6°, 50.9°, and 74.7° are ascribed to the (111), (002), and (022) planes of Cu, while the 44.5°, 51.9°, and 76.4° are the (111), (200), and (220) planes of Ni.[27] Thereby, the conjugated acetylenic polymers were successfully grown on both supports (1×3 cm^2), Cu foams (CAPs/Cu), and Ni foams (CAPs/NiCu) for HER and OER investigations, respectively. The same XPS patterns were detected for the CAPs grown on both supports (Figure S11). As shown in the linear sweep voltammetry (LSV) under simulated-solar light illumination, the collected negative photocurrents reveal that the HER is still occurring under oxidative potentials (Figure 2a). Interestingly, at V = 0.93 V (vs. RHE), hereby defined as inversion potential (E_{inv}) the photocurrent is equal to 0. The OER only begins to occur at a bias higher than E_{inv} (Figure 2b). Under solar illumination, **pTET**/NiCu exhibited a remarkable OER photocurrent density of ~200 μA cm^{-2} at 1.23 V vs. RHE. On the other hand, **pTEB**/NiCu and **pTETH**/NiCu provided values of only ~80 and ~50 μA cm^{-2}, respectively. As a control experiment, the NiCu foam displayed negligible photo response (as low as 5 μA cm^{-2} at 1.23 V vs. RHE; Figure S12).

The long-term performance displayed by **pTET**/NiCu was also measured. After ca. 1.75 h of continuous operation, the photoelectrode can still produce oxygen under the reapplication of light (Figure S13). It should be noted that the photocurrent generated by **pTET**/NiCu outperforms the previously reported co-catalysts free fluorene-dibenzothiophene-S,S-dioxide-containing polymers (1.1–32.5 μA cm^{-2} at pH 7),[28] pTEB/ITO (7.5 μA cm^{-2} at pH 13),[29] and even some carbon nitride-based materials (72 and 103.2 μA cm^{-2} at pH 13 and 6.5, respectively).[30–31] In addition, the evolved oxygen product generated from **pTET** was analysed using a gas chromatograph (GC) coupled with a TCD detector, revealing a Faraday efficiency (FE) of almost 95%. Moreover, the charge separation efficiency (P_{cs}) was measured according to the equation:[32] $J_{ph} = J_{abs} \times P_{cs} \times P_{ci}$, where J_{ph} is the total photocurrent density, J_{abs} is the photon absorption rate, P_{cs} is the charge separation efficiency, and P_{ci} is the charge injection yield to the electrolyte. At 1.23 V vs. RHE, **pTET** showed a charge separation efficiency of 56.7%, which is 2.23 and 6.7 times higher than **pTEB** (26.7%) and **pTETH** (8.42%), respectively (Figure 2c). The increasing donor-acceptor character is the key parameter for the superior OER performance displayed by **pTET**.

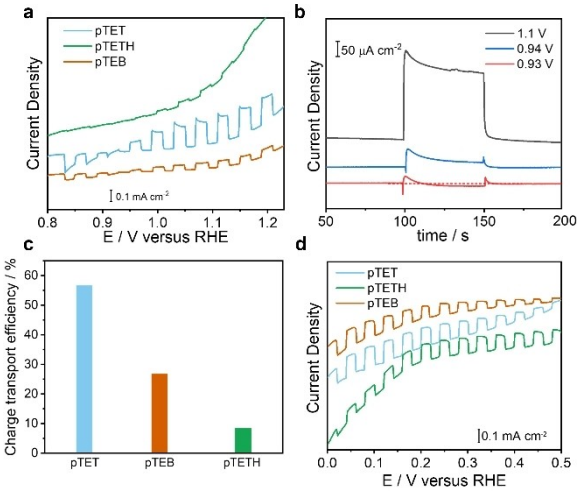

Figure 2. Photoelectrochemical tests. a) Linear Sweep Voltammetry of the CAPs/NiCu recorded at 2 mVs^{-1} in 0.1 M KOH (pH 13). b) Amperometric responses of **pTET**/NiCu at different applied bias (vs. RHE). c) Charge transport efficiency at 1.23 V vs. RHE. d) Linear Sweep Voltammetry of the CAPs/Cu recorded at 2 mVs^{-1} in 0.1 M Na_2SO_4 (pH 6.8).

Next, the PEC HER performance of the CAPs/Cu foam was assessed in neutral medium (pH 6.8). The bare Cu foam (support) was already known not to show any HER performance in neutral conditions.[21] LSV and amperometric measurements revealed the following performance trend (at 0.3 V vs. RHE): **pTET** > **pTEB** > **pTETH**. Apparently, the introduction of the triazine ring in the polymer backbone of **pTET** was beneficial for the HER performance, leading to the highest photocurrent density of ~190 μA cm^{-2} at 0.3 V vs. RHE (Figure 2d and Figure S14), which is comparable (or higher) with the state of the art co-catalysts-free organic photocathodes in neutral medium, such as CuO_4-linked arylene-ethynylene two dimensional conjugated MOF[33] (260 μA cm^{-2} at 0.3 V vs. RHE), thiophene-bridged sp^2-carbon linked 2D conjugated polymers[34] (7.9 μA cm^{-2} at 0.3 V vs. RHE), and other CAPs[35] (55 μA cm^{-2} at 0.3 V vs. RHE) as well. Moreover, GC measurements validated a H_2 FE higher than 95%. Additionally, electrochemical impedance spectroscopy (EIS) was conducted to reveal the charge transfer resistance of the CAPs under light illumination. The following trend (with and without illumination, at 0.3 V vs. RHE) was observed: **pTET** < **pTETH** < **pTEB**, with **pTETH** undergoing the most drastic change under light irradiation (Figure S15 and Table S1). The demonstrated ability of **pTET** to perform both the water splitting reactions will be further explored in the future work when the catholyte (pH 6.8) and the anolyte (pH 13) compartments will be connected by a bipolar membrane[36–37] in order to assess its overall water splitting ability.

Theoretical investigations were subsequently performed to reveal the catalytic active sites of **pTET** for both HER and OER reactions.[38–39] All the possible adsorption sites (labelled 1–8) were examined (Figure 3a). As revealed by the HER free-energy diagram at 0 V vs. RHE (at pH 6.8), the most active atoms are the C_{sp} of the triple bond linkages (atom 7) and the N atom of the triazine ring with a relative energy difference of 0.03 eV upon light irradiation (U_e = 0.64 V; Figure 3b). The anodic reaction was also investigated. As known, the OER can proceed with two different mechanisms, namely via the single- and the dual-site processes (Eq. S4.1-S4.7). As it is a multistep reaction, the overpotential (η), defined as $\eta = \Delta G_{RDS} - E^0_{OER}$ where ΔG_{RDS} is ΔG of the rate-determining step (RDS) and E^0_{OER} is the water oxidation equilibrium potential (0.46 V at pH 13), describes the efficiency of each active site. For the single-site process, the RDS was calculated to be the conversion from O* to OOH* due to the high-energy barrier. Without light irradiation, the overpotential for the most active sites 7 and 8, are 1.5 eV and 1.29 eV, respectively. Upon light irradiation (U_h = 2.05 V), their

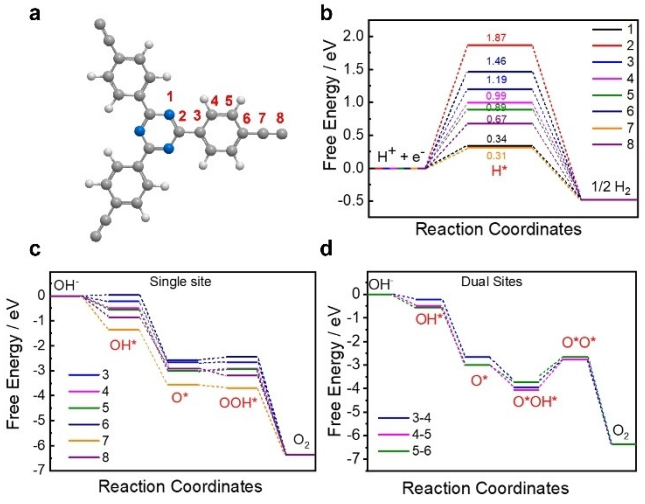

Figure 3. DFT Simulations to investigate the active sites in **pTET**. a) Chemical Structure with corresponding atom numbers (grey sphere are for carbon, blue for nitrogen, and white for hydrogen). b) Free-energy diagram for the H_2 evolution via Holmer-Heyrovsky pathway at 0 V vs. RHE and pH 6.8, under light irradiation ($U_e = 0.64$ V), for all the possible catalytic sites. Free-energy diagram for O_2 evolution via c) single site mechanism, and d) dual sites mechanism at 1.23 V vs. RHE and pH 13, under light irradiation ($U_h = 2.05$ V), for all the possible catalytic sites.

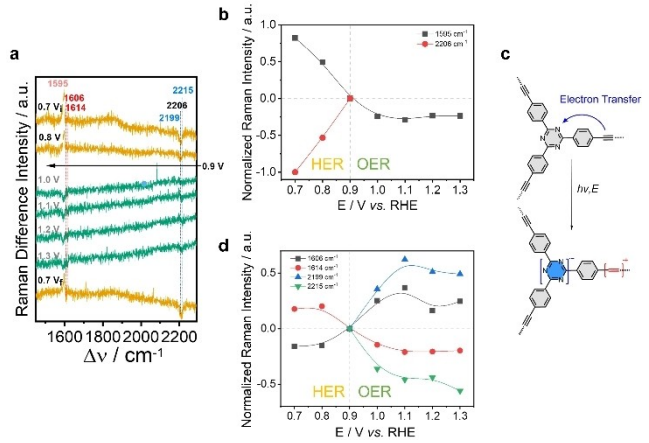

Figure 4. Electrochemical-operando Resonance Raman of **pTET**/NiCu under 594 nm laser irradiation (0.1 M KOH). a) Potential-dependent difference Raman spectra. The spectra are against the spectrum collected at 0.9 V; V_i and V_f are the initial and final spectra, respectively. b) Potential-dependent difference intensities of the 1595 and 2206 cm^{-1}. c) Schematics of the proposed reaction intermediate. d) Potential-dependent difference intensities of the 1606, 1641, 2199, and 2215 cm^{-1}.

free-energy diagrams go downhill (Figure 3c), indicating that the OER single-site process can occur spontaneously under light irradiation. Due to the similar chemical environment, only the pairs 3–4, 4–5, and 5–6 can undergo dual-site OER, with η of 0.88, 1.16, and 0.86 eV, respectively, which are much higher than the single-site process (Figure 3d). Electrochemical-operando RR spectroscopy was further performed to obtain mechanistic insights and to detect catalytic intermediates in **pTET**.[40] In this setup configuration, the irradiation laser initiates the PEC process and simultaneously allows the acquisition of the Raman spectrum of the reactive interface (Figure S16).[41]

As depicted in Figure 4a, the potential-dependent difference Raman spectra of **pTET**/NiCu (vs. 0.9 V~E_{inv}) showed two different trends: the first one (HER range, yellow spectra) goes from 0.7 to 0.8 V vs. RHE and the second one from 1.0 to 1.3 V vs. RHE (OER range, in green). At HER potentials, the difference Raman spectra displayed an apparent increase and decrease in intensity of the 1595 cm^{-1} and 2206 cm^{-1} peaks, respectively (Figure 4b). Such a correspondence points to an electron transfer from the electron-rich triple bonds to the electron-accepting triazine units of **pTET**, leaving the sp linkages in a sp^2 double bond-like intermediate (Figure 4c). Subsequently, the electron-enriched N-atoms of the triazine moieties become active sites for the HER, which is in agreement with the literature[19] and our DFT calculations. In the second step, electrons delivered from the electrode re-establish the triple bond. The visibility of the intermediate band (at 1595 cm^{-1}) in the Raman spectra suggests that the back-reduction of the triple bond is the RDS of the whole catalytic cycle. Above the inversion potential, drastic spectral changes are clearly visible in the RR difference spectra. In the OER region (green spectra), two downshift bands 1614→1606 cm^{-1} and 2214→2199 cm^{-1} can be visualized in the potential-dependent difference plot (Figures 4d, S17-18), with the maximum at ~1.1 V corresponding to the highest photocurrent collected under solar-simulated light. Furthermore, the HER under neutral conditions was also studied with electrochemical RR spectroscopy (Figure S19).

Based on the above observations, we propose the following catalytic mechanisms for the two half reactions on **pTET**. The HER occurs as follows: (1) a photoinduced electron transfer enriches the N atoms of the triazine rings, leaving the triple bonds in a sp^2-like state. This allows the (2) first protonation (Volmer step) to occur on the N atoms, while the hydrogen release proceeds via a Heyrovsky step (3). The catalyst is then restored to the ground state (4) via an electron transfer from the underlying metallic Cu foam. Schematics of the energy levels are sketched in Figure 5b, where the Cu foam energy level corresponds to the Fermi level, obtained from UPS. Besides, the OER can occur via two different pathways. The single site (Figure 5c) occurs with the (1) first hydroxide addition to the sp-carbon (atom 5), followed by the O* formation (2). The formation of the peroxide intermediate (3) is also the RDS of the catalytic process, with the fourth hydroxide addition leading to the oxygen release. The dual-site mechanism (Figure 5d) is proposed to start with a (1) photo-induced charge transfer from the C4-C5 to the C5-C6 bonds of the (4-ethynylphenyl) units of **pTET**. It is then followed by the bonding of the first hydroxide (2) on atom 5 and the formation of the epoxide-like intermediate between atoms 4 and 5 (after the second hydroxide bonding) (3). The catalysis proceeds with the third oxidation (4) on atom 6, paving the way for the hydroperoxide (O–O)* species (5), which is also the RDS of the catalytic cycle. The following spontaneous oxygen release (6) brings the catalyst back to the ground state.

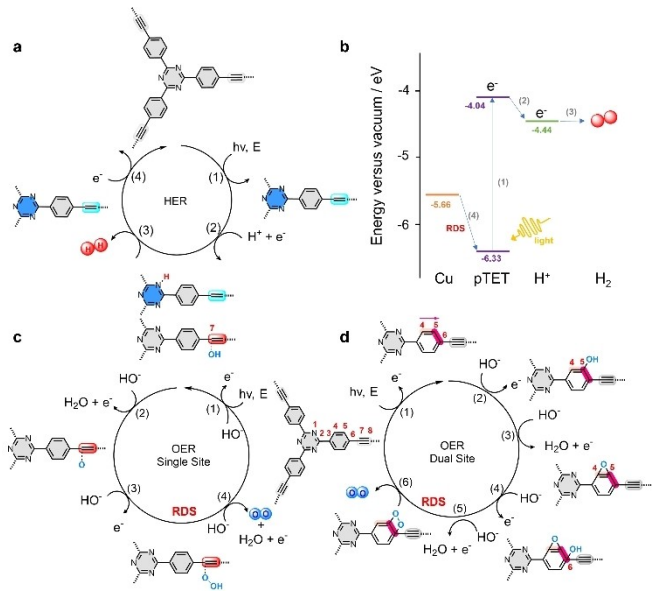

Figure 5. Proposed Mechanisms. a) HER proposed mechanism. b) Schematics for the energy levels. c) OER Single Site mechanism, and d) OER dual site mechanism.

Conclusions

In this work, we demonstrated the first example of donor-acceptor conjugated polymers that can be employed as both photocathode and photoanode. Among them, under simulated solar light illumination, **pTET**, with the highest donor-acceptor character, reports impressive OER and HER photocurrents of ~200 μA cm−2 at 1.23 V vs. RHE (at pH 13) and ~190 μA cm−2 at 0.3 V vs. RHE (at pH 6.8), respectively. Mechanistic insights were carried out by combining electrochemical-operando RR spectroscopy and DFT calculations. We propose that the HER occurs via a photoinduced electron transfer from the triple bonds to the triazine moieties of **pTET**, turning them into HER active sites, while the OER can occur on both the electron-depleted triple bonds and on the C5-C6 of the (4-ethynylphenyl) units of **pTET**. We believe that our work will contribute to further exploring and designing novel high-performance organic-based photoelectrodes not only for water splitting but also for other photoelectrocatalytic processes (e.g., N_2 reduction and CO_2 fixation).

Supporting Information

The authors have cited additional references within the Supporting Information (Refs. [42–51]).

Acknowledgements

M.B., Y.A., and C.J.Q. contributed equally to this work. This work was financially supported by the Graphene Flagship (GrapheneCore3, No. 881603), the cluster of excellence UniSysCat (EXC 2008/1-390540038), the Sächsisches Staatsministerium für Wissenschaft und Kunst (Projekt SEALEC), and the Deutsche Forschungsgemeinschaft (CRC1415: 417590517). We acknowledge the cfaed (Center for Advancing Electronics Dresden) and the Dresden Center for Nano-analysis (DCN) at TU Dresden. A.T. and C.N. acknowledge DFG TRR 234 "Catalight" (B7 and Z2) and research infrastructure grant INST 275/257-1. Y. An and A. Kuc acknowledge the High-Performance Computing (ZIH) at TU Dresden for computing resources. H.S. acknowledges the National Natural Science foundation China (22209076), the Natural Science Foundation of Jiangsu Province (Grant No. BK 20220369), and the Jiangsu Specially Appointed Professorship.We acknowledge Li Li for GC measurements.. Open Access funding enabled and organized by Projekt DEAL.

Conflict of Interests

The authors declare no conflict of interest.

Data Availability Statement

The data that support the findings of this study are available from the corresponding author upon reasonable request.

Keywords: bifunctional photoelectrodes · oxygen evolution · hydrogen evolution · resonance Raman · conjugated polymers

[1] N. Armaroli, V. Balzani, *Angew. Chem. Int. Ed.* **2007**, *46*, 52–66.
[2] M. Grätzel, *Nature* **2001**, *414*, 338–344.
[3] N. Armaroli, V. Balzani, *ChemSusChem* **2011**, *4*, 21–36.
[4] A. Fujishima, K. Honda, *Nature* **1972**, *238*, 37–38.
[5] A. Landman, H. Dotan, G. E. Shter, M. Wullenkord, A. Houaijia, A. Maljusch, G. S. Grader, A. Rothschild, *Nat. Mater.* **2017**, *16*, 646–651.
[6] A. Paracchino, V. Laporte, K. Sivula, M. Grätzel, E. Thimsen, *Nat. Mater.* **2011**, *10*, 456–461.
[7] C. G. Morales-Guio, S. D. Tilley, H. Vrubel, M. Grätzel, X. Hu, *Nat. Commun.* **2014**, *5*, 3059.
[8] P. Dai, W. Li, J. Xie, Y. He, J. Thorne, G. McMahon, J. Zhan, D. Wang, *Angew. Chem.* **2014**, *126*, 13711–13715.
[9] C. Li, T. Hisatomi, O. Watanabe, M. Nakabayashi, N. Shibata, K. Domen, J. J. Delaunay, *Energy Environ. Sci.* **2015**, *8*, 1493–1500.
[10] X. Yu, M. S. Prévot, N. Guijarro, K. Sivula, *Nat. Commun.* **2015**, *6*, 1–8.
[11] J. R. McKone, A. P. Pieterick, H. B. Gray, N. S. Lewis, *J. Am. Chem. Soc.* **2013**, *135*, 223–231.
[12] J. Luo, L. Steier, M. K. Son, M. Schreier, M. T. Mayer, M. Grätzel, *Nano Lett.* **2016**, *16*, 1848–1857.
[13] W. Septina, Gunawan, S. Ikeda, T. Harada, M. Higashi, R. Abe, M. Matsumura, *J. Phys. Chem. C* **2015**, *119*, 8576–8583.
[14] J. W. Jang, C. Du, Y. Ye, Y. Lin, X. Yao, J. Thorne, E. Liu, G. McMahon, J. Zhu, A. Javey, J. Guo, D. Wang, *Nat. Commun.* **2015**, *6*, 1–5.
[15] Y.-H. Lai, D. W. Palm, E. Reisner, Y.-H. Lai, D. W. Palm, E. Reisner, *Adv. Energy Mater.* **2015**, *5*, 1501668.
[16] L. Pan, J. H. Kim, M. T. Mayer, M. K. Son, A. Ummadisingu, J. S. Lee, A. Hagfeldt, J. Luo, M. Grätzel, *Nat. Catal.* **2018**, *1*, 412–420.
[17] S. Ida, K. Yamada, T. Matsunaga, H. Hagiwara, Y. Matsumoto, T. Ishihara, *J. Am. Chem. Soc.* **2010**, *132*, 17343–17345.
[18] S. Otep, T. Michinobu, Q. Zhang, *Solar RRL* **2020**, *4*, 1900395.
[19] Y. Zhang, H. Lv, Z. Zhang, L. Wang, X. Wu, H. Xu, *Adv. Mater.* **2021**, *33*, 2008264.
[20] J. Cornil, J. L. Brédas, J. Zaumseil, H. Sirringhaus, *Adv. Mater.* **2007**, *19*, 1791–1799.
[21] H. Sun, I. H. Öner, T. Wang, T. Zhang, O. Selyshchev, C. Neumann, Y. Fu, Z. Liao, S. Xu, Y. Hou, A. Turchanin, D. R. T. Zahn, E. Zschech, I. M.

Weidinger, J. Zhang, X. Feng, *Angew. Chem. Int. Ed.* **2019**, *58*, 10368–10374.
[22] M. Borrelli, C. J. Querebillo, D. L. Pastoetter, T. Wang, A. Milani, C. Casari, H. K. Ly, F. He, Y. Hou, C. Neumann, A. Turchanin, H. Sun, I. M. Weidinger, X. Feng, *Angew. Chem. Int. Ed.* **2021**, *60*, 18876–18881.
[23] T. Zhang, Y. Hou, V. Dzhagan, Z. Liao, G. Chai, M. Löffler, D. Olianas, A. Milani, S. Xu, M. Tommasini, D. R. T. Zahn, Z. Zheng, E. Zschech, R. Jordan, X. Feng, *Nat. Commun.* **2018**, *9*, 1140.
[24] Y. Xin, K. Yu, L. Zhang, Y. Yang, H. Yuan, H. Li, L. Wang, J. Zeng, Y. Xin, K. Yu, L. Zhang, Y. Yang, H. Yuan, L. Wang, H. Li, J. Zeng, *Adv. Mater.* **2021**, *33*, 2008145.
[25] S. D. Giri, A. Sarkar, *J. Electrochem. Soc.* **2016**, *163*, H252–H259.
[26] N. Lotfi, T. Shahrabi, Y. Yaghoubinezhad, G. B. Darband, *J. Electroanal. Chem.* **2019**, *848*, 113350.
[27] X. Hu, X. Tian, Y. W. Lin, Z. Wang, *RSC Adv.* **2019**, *9*, 31563–31571.
[28] C. Dai, X. Gong, X. Zhu, C. Xue, B. Liu, *Mater. Chem. Front.* **2018**, *2*, 2021–2025.
[29] S. Jayanthi, D. V. S. Muthu, N. Jayaraman, S. Sampath, A. K. Sood, *ChemistrySelect* **2017**, *2*, 4522–4532.
[30] G. Peng, J. Albero, H. Garcia, M. Shalom, *Angew. Chem. Int. Ed.* **2018**, *57*, 15807–15811.
[31] Q. Ruan, W. Luo, J. Xie, Y. Wang, X. Liu, Z. Bai, C. J. Carmalt, J. Tang, *Angew. Chem. Int. Ed.* **2017**, *56*, 8221–8225.
[32] H. Dotan, K. Sivula, M. Grätzel, A. Rothschild, S. C. Warren, *Energy Environ. Sci.* **2011**, *4*, 958–964.
[33] Y. Lu, H. Zhong, J. Li, A. M. Dominic, Y. Hu, Z. Gao, Y. Jiao, M. Wu, H. Qi, C. Huang, L. J. Wayment, U. Kaiser, E. Spiecker, I. M. Weidinger, W. Zhang, X. Feng, R. Dong, *Angew. Chem. Int. Ed.* **2022**, *61*, e202208163.
[34] S. Xu, H. Sun, M. Addicoat, B. P. Biswal, F. He, S. Park, S. Paasch, T. Zhang, W. Sheng, E. Brunner, Y. Hou, M. Richter, X. Feng, *Adv. Mater.* **2021**, *33*, 2006274.
[35] H. Sun, C. Neumann, T. Zhang, M. Löffler, A. Wolf, Y. Hou, A. Turchanin, J. Zhang, X. Feng, *Adv. Mater.* **2019**, *31*, 1900961.
[36] D. A. Vermaas, M. Sassenburg, W. A. Smith, *J. Mater. Chem. A* **2015**, *3*, 19556–19562.
[37] J. Luo, D. A. Vermaas, D. Bi, A. Hagfeldt, W. A. Smith, M. Grätzel, *Adv. Energy Mater.* **2016**, *6*, 1600100.
[38] B. Hinnemann, P. G. Moses, J. Bonde, K. P. Jørgensen, J. H. Nielsen, S. Horch, I. Chorkendorff, J. K. Nørskov, *J. Am. Chem. Soc.* **2005**, *127*, 5308–5309.
[39] A. Kulkarni, S. Siahrostami, A. Patel, J. K. Nørskov, *Chem. Rev.* **2018**, *118*, 2302–2312.
[40] H. K. Ly, I. Weidinger, *Chem. Commun.* **2021**, *57*, 2328–2342.
[41] Y. Liu, M. Bouri, L. Yao, M. Xia, M. Mensi, M. Grätzel, K. Sivula, U. Aschauer, N. Guijarro, *Angew. Chem. Int. Ed.* **2021**, *60*, 23651–23655.

Manuscript received: November 20, 2023
Accepted manuscript online: December 8, 2023
Version of record online: ■■, ■■

RESEARCH ARTICLE

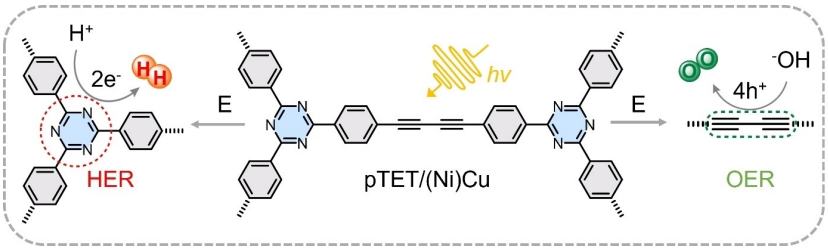

By a careful design of monomers and supports, we demonstrate that donor-acceptor conjugated acetylenic polymers (CAPs) can produce, under light irradiation and electrochemical bias, both hydrogen and oxygen, in neutral and alkaline solutions, respectively.

Dr. M. Borrelli, Dr. Y. An, Dr. C. J. Querebillo, Dr. A. Morag, Dr. C. Neumann, Prof. Dr. A. Turchanin, Prof. Dr. H. Sun, Dr. A. Kuc, Prof. Dr. I. M. Weidinger, Prof. Dr. X. Feng**